

# A North America Wide Area Neutral Atmosphere Model for GNSS Applications

RODRIGO F. LEANDRO,<sup>1,2</sup> MARCELO C. SANTOS,<sup>1</sup> and RICHARD B. LANGLEY<sup>1</sup>

<sup>1</sup>Geodetic Research Laboratory, Department of Geodesy and Geomatics Engineering,  
University of New Brunswick, Fredericton, Canada

<sup>2</sup>Trimble Terrasat GmbH, Trimble Geomatics and Engineering Group, Hoehenkirchen, Germany

*Received August 2007; Revised January 2009*

**ABSTRACT:** *In this paper we are introducing a new neutral atmosphere model, which was designed to provide better predictions for different regions inside a delimited wide area. The goal of this new development is to have a more reliable model for wide area augmentation system users, with some homogeneity in terms of accuracy performance over the area of interest. The approach for creating the new wide area neutral atmosphere model for North America (UNBw.na) is comprehensively described and discussed. All result analyses took into consideration the most recent version of the UNB models, until now, UNB3m. Results for prediction of meteorological parameters show that the new grid-based model can perform better than a latitude (only) based model (such as UNB3m). The analyses showed that UNBw.na is consistently better than UNB3m in several aspects, and the adopted procedure for a meteorological parameter grid calibration has resulted in a reliable model.*

## INTRODUCTION

Mitigating neutral atmosphere refraction is a crucial step in GNSS positioning. Often called tropospheric delays, the neutral atmosphere delays are one of the main sources of measurement error in global navigation satellite systems (GNSS). A typical way to account for these effects is by using prediction models. There are also other alternatives for neutral atmosphere delay mitigation, such as the parameterization of the zenith delay in the positioning model, when dual frequency carrier-phase measurements are available. However, even in this case, the parameter is commonly a residual delay to correct the initially predicted delay, which means that a prediction model is also needed. In most GNSS applications the prediction of the neutral atmosphere delay is required, even if only for an initial value for which a residual delay is computed.

In this paper we discuss developments related to neutral atmosphere delay prediction models at the University of New Brunswick (UNB). A number of UNB models have been developed over the past decade. Our penultimate model is called UNB3m and a comprehensive description of it can be found in previous publications [1, 2].

UNB neutral atmosphere models have their algorithm based on the prediction of surface meteorological parameter values, which are used to compute hydrostatic and non-hydrostatic zenith delays for a site using the modified Saastamoinen models [3]. The slant delays are determined by applying the Niell mapping functions [4] to the zenith delays.

In order to account for the seasonal and regional variation of the neutral atmosphere's behavior, meteorological parameters (barometric pressure ( $P$ ), temperature ( $T$ ), relative humidity ( $RH$ ), temperature lapse rate ( $\beta$ ), and water vapor pressure height factor ( $\lambda$ )) are used as functions of time (day of year) and geographical location in UNB models. Each meteorological parameter is modeled with two components: the average (mean) and amplitude of a cosine function with a one year period. By definition, the origin of the yearly variation is day of year 28. This procedure is similar to the one used in the computations of the Niell mapping functions.

After the average and amplitude of a given meteorological parameter are determined, the parameter value is estimated for the desired day of year according to:

$$X_{doy} = Avg - Amp \cdot \cos\left((doy - 28) \frac{2\pi}{365.25}\right), \quad (1)$$

Table 1—Look-Up Table of UNB3m Model

Average					
Latitude (degrees)	Pressure (mbar)	Temperature (K)	RH (%)	$\beta$ (K m <sup>-1</sup> )	$\lambda$ (unitless)
15	1013.25	299.65	75.0	6.30e-3	2.77
30	1017.25	294.15	80.0	6.05e-3	3.15
45	1015.75	283.15	76.0	5.58e-3	2.57
60	1011.75	272.15	77.5	5.39e-3	1.81
75	1013.00	263.65	82.5	4.53e-3	1.55

Amplitude					
Latitude (degrees)	Pressure (mbar)	Temperature (K)	RH (%)	$\beta$ (K m <sup>-1</sup> )	$\lambda$ (unitless)
15	0.00	0.00	0.0	0.00e-3	0.00
30	-3.75	7.00	0.0	0.25e-3	0.33
45	-2.25	11.00	-1.0	0.32e-3	0.46
60	-1.75	15.00	-2.5	0.81e-3	0.74
75	-0.50	14.50	2.5	0.62e-3	0.30

where  $X_{doy}$  represents the computed parameter value for day of year (*doy*), and *Avg* and *Amp* are the average and amplitude values, respectively. This procedure is followed for each of the previously mentioned five parameters.

Once all parameters are determined for a given location and day of year, the zenith delays (in meters) are computed according to:

$$d_h^z = \frac{10^{-6}k_1R}{g_m} \cdot P_0 \cdot \left(1 - \frac{\beta H}{T_0}\right)^{\frac{g}{R\beta}}, \quad (2)$$

and

$$d_{nh}^z = \frac{10^{-6}(T_m k'_2 + k_3)R}{g_m \lambda' - \beta R} \cdot \frac{e_0}{T_0} \cdot \left(1 - \frac{\beta H}{T_0}\right)^{\frac{\lambda' g}{R\beta} - 1}, \quad (3)$$

where

- $d_h^z$  and  $d_{nh}^z$  are the hydrostatic and non-hydrostatic zenith delays, respectively;
- $T_0$ ,  $P_0$ ,  $e_0$ ,  $\beta$ , and  $\lambda$  are the meteorological parameters computed according to (1), where the subscript 0 indicates mean sea level;
- $H$  is the orthometric height of the site in meters;
- $R$  is the gas constant for dry air (287.054 J kg<sup>-1</sup>K<sup>-1</sup>);
- $g_m$  is the acceleration of gravity at the atmospheric column centroid in m s<sup>-2</sup> and can be computed from

$$g_m = 9.784(1 - 2.66 \times 10^{-3} \cos(2\phi) - 2.8 \times 10^{-7} H); \quad (4)$$

- $g$  is the standard acceleration of gravity (9.80665 m s<sup>-2</sup>);
- $T_m$  is the mean temperature of water vapor in kelvins and can be computed from

$$T_m = (T_0 - \beta H) \left(1 - \frac{\beta R}{g_m \lambda'}\right) \quad (5)$$

- $\lambda' = \lambda + 1$  (unitless); and,
- $k_1$ ,  $k'_2$ , and  $k_3$  are refractivity constants with values 77.60 K mbar<sup>-1</sup>, 16.6 K mbar<sup>-1</sup>, and 377600 K<sup>2</sup> mbar<sup>-1</sup>, respectively.

The total slant delay is computed according to

$$d_t = m_h d_h^z + m_{nh} d_{nh}^z, \quad (6)$$

where  $m_h$  and  $m_{nh}$  stand for hydrostatic and non-hydrostatic Niell mapping functions, respectively.

The procedure above has been used in all versions of UNB models, with the differences among them depending on the way the meteorological parameters ( $T_0$ ,  $P_0$ ,  $e_0$ ,  $\beta$ , and  $\lambda$ ) are determined. Other models have also been based on the same principles, such as the Galileo System Test Bed models developed by the European Space Agency [5]. In the case of UNB3m, a look-up table with average and amplitude of the meteorological parameters derived from the U.S. Standard Atmosphere Supplements, 1966 [6] is used. Table 1 shows the UNB3m look-up table.

Using the table above, UNB3m is able to predict total zenith delays with an average rms of 4.9 cm [1]. Previous analysis showed that this rms value likely could be improved if more realistic meteorological parameter values were used. Collins and Langley [7] showed that if UNB models are used with surface-measured meteorological values, they can provide delays with an average uncertainty of around 3.5 cm, which would be the performance of a UNB neutral atmosphere model if a perfect surface meteorology model could be implemented. Based on these numbers it is possible to state that a better model than the currently used UNB3m

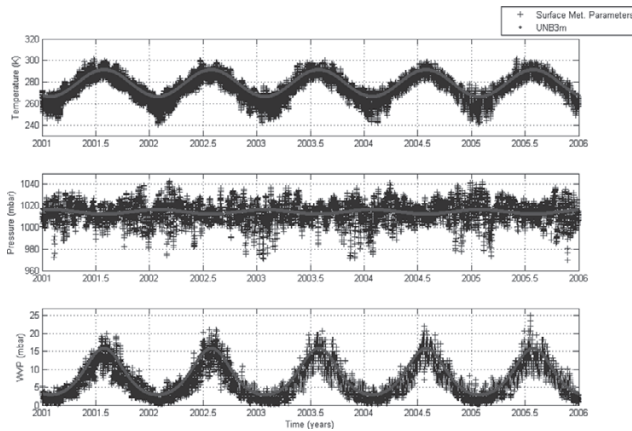


Fig. 1—UNB3m surface meteorological parameter predictions compared to measured surface parameter values.

could provide zenith delays with uncertainties between 3.5 and 4.9 cm. One of the reasons why UNB3m is not capable of predicting delays with uncertainty close to 3.5 cm is the fact that the current look-up table is not able to accommodate the differences in the average surface meteorology of different regions. Part of this modeling inability is also due to day-to-day variation of meteorological parameters.

However, this variation impacts any prediction model, since the modeled behavior is always a smooth curve in time (in our case a cosine curve over the year) while real values are points scattered about this line. Figure 1 shows the day-to-day variation over several years for a station situated at approximately 50° N, 66° W. The crosses are the surface measurements of temperature, pressure, and water vapor pressure, and the dots are the predicted values using UNB3m. The meteorological measurements came from the Integrated Surface Hourly Database, which will be discussed later in this paper.

The advantage of having a more realistic UNB model with the same functional model as UNB3m is in the values of the yearly averages and amplitudes, as well as their geographical variation. This is the motivation for creating a new model, capable of describing the behavior of meteorological values more realistically.

UNB neutral atmosphere models have been used extensively in the context of SBAS (Satellite Based Augmentation Systems). This is the case of CDGPS (Canada-wide Differential GPS), which recommends the use of the UNB3 model by the users, WAAS (Wide Area Augmentation System) and WAAS compatible systems, which use a modified version of the UNB3 model running in all WAAS-capable receivers. Although UNB3 is currently the most widely used version of UNB models, the most recent one that has been made available is

UNB3m, which offers a significant improvement in terms of non-hydrostatic zenith delay prediction compared to its predecessor.

In this paper we are introducing a new model, which was designed to provide better predictions for different regions inside a delimited wide area. The goal is to have a more reliable model for wide area augmentation system users, with some homogeneity in terms of performance over the area of interest. These new models are called here wide area neutral atmosphere models and are treated in more detail in the next section.

## WIDE AREA MODELS

In this section, the way in which the wide area models are generated is reviewed. The first important characteristic of these models is that they keep the same physical assumptions as before (Equations (1) to (6)). The key difference in the new approach is the way site meteorological values are evaluated, in this case, using a two-dimensional grid table instead of a latitude-band look-up table.

One of the first aspects to be taken into account when generating a new model is the data available for its calibration. In this work, we used a data set with world-wide hourly measurements of surface temperature, surface dew point temperature, and mean sea level (MSL) barometric pressure. The measurements were made between the years of 2001 and 2005, inclusive. This dataset was provided by the U.S. National Oceanic and Atmospheric Administration (NOAA), from its Integrated Surface Hourly (ISH) Database. Figure 2 shows the global distribution of the ISH Database, a total of 17,415 stations.

The observations of surface temperature, dew point temperature, and MSL pressure are used to calibrate a grid with values of average and

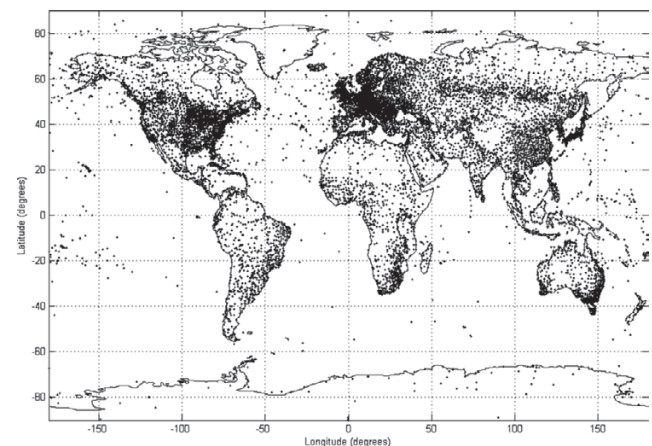


Fig. 2—Distribution of ISH Database meteorological stations.

amplitude (to be used as in Equation (1)) for each of the three parameters. In the case of dew point temperature, it is converted to relative humidity (this conversion is discussed later in this section). Near surface temperature lapse rate and water vapor pressure height factor parameters can also be computed if desired. The functional model used for the grid interpolation is a very simple bilinear model, based on the four nearest grid nodes to the observation point (in the case of grid calibration) or prediction point (in the case of grid use). The value of interest can be computed according to the following formula:

$$X = (1-p)(1-q)x_1 + p(1-q)x_2 + q(1-p)x_3 + pqx_4, \quad (7)$$

where  $X$  is the computed value (it is either the average or amplitude of one of the modeled parameters),  $x_i$  is the parameter value at grid node  $i$ , and  $p$  and  $q$  are as shown in Figure 3.

In Figure 3,  $Dx$  and  $Dy$  represent the grid spacing in longitude and latitude, respectively. The black square in the middle of the grid represents the observation point, with coordinates  $\phi_{point}$  and  $\lambda_{point}$ . The values for  $p$  and  $q$  can be computed as:

$$p = (\lambda_{point} - \lambda_1)/Dx, \quad (8)$$

and

$$q = (\phi_{point} - \phi_1)/Dy, \quad (9)$$

where  $\lambda_1$  and  $\phi_1$  are the longitude and latitude of grid node 1 (as represented in Figure 3, where the numbers 1 to 4 indicate the position of the respective  $i^{th}$  grid node). Therefore,  $p$  and  $q$  can assume values between 0 and 1.

Once all site meteorological parameters for the point of interest are determined using the procedure above, the neutral atmosphere delays can be

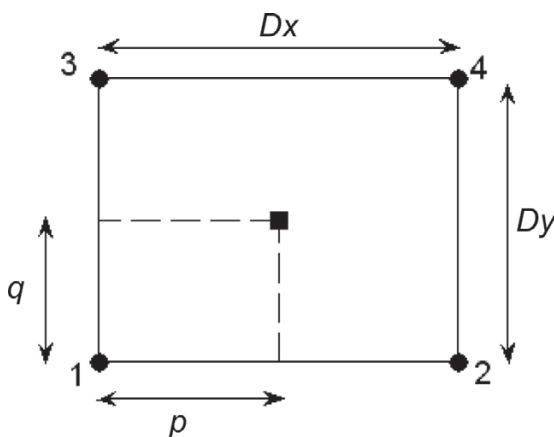


Fig. 3—Grid interpolation procedure.

estimated using Equations (1) to (6). As can be seen, the use of the grid does not bring any significant complexity to the user. However, the grid generation is not a simple procedure.

The establishment of the values for each grid node is carried out in three steps. The first one is the calibration of the temperature ( $T$ ) grid, followed by pressure ( $P$ ) and relative humidity ( $RH$ ) grids. The computation is performed on a station-by-station basis, where all data (all measurements over the observed years) is processed at each station step. For each station, the computation is performed on a year-by-year basis. This procedure is used to improve processing time, since the amount of data is too large to be processed in one single batch adjustment. The general least-squares adjustment model (used in all three grid calibrations) is:

$$\mathbf{x} = \mathbf{x}_0 + \left( \mathbf{A}^t \mathbf{C}_\ell^{-1} \mathbf{A} + \mathbf{N}_p \right)^{-1} \mathbf{A}^t \mathbf{C}_\ell^{-1} \mathbf{w}, \quad (10)$$

where  $\mathbf{x}$  is the vector of updated parameters (i.e., the values of the gridded parameters at the grid nodes),  $\mathbf{x}_0$  is the vector of *a priori* parameters (coming from previous updates),  $\mathbf{A}$  is the design matrix,  $\mathbf{C}_\ell^{-1}$  is the observation weight matrix,  $\mathbf{N}_p$  is the parameter normal matrix (coming from previous updates) and  $\mathbf{w}$  is the misclosure vector. The parameter normal matrix gets updated at each step, as follows:

$$\mathbf{N}_{pu} = \left( \mathbf{A}^t \mathbf{C}_\ell^{-1} \mathbf{A} + \mathbf{N}_{p0} \right), \quad (11)$$

where  $\mathbf{N}_{pu}$  is the updated normal matrix and  $\mathbf{N}_{p0}$  is the *a priori* normal matrix. At each update of the filter, Equations (10) and (11) are evaluated. The current normal matrix is used as  $\mathbf{N}_p$  in (10), and then used as  $\mathbf{N}_{p0}$  in (11), and after this  $\mathbf{N}_{pu}$  becomes the current normal matrix until another filter update is performed. The observations involved in each update step are the surface meteorological measurements for the current station and current year. The parameters are adjusted for the four nearest grid nodes, using the same functional model as in (7). Therefore, the functional model in the adjustment of each grid type ( $T$ ,  $P$ ,  $RH$ ) is built considering (7) plus the relevant formulas (relating interpolated grid values to measurements) for the given parameter type.

The first step, the temperature grid generation, involves the adjustment of values for MSL temperature and optionally the temperature lapse rate. In case the lapse rates are not being adjusted, *a priori* values from UNB3m are used as known values. The basic functional model for this step is given by:

$$T = T_0 - \beta H, \quad (12)$$

or, introducing the yearly variation:

$$T = \left( T_{avg} - T_{amp} \cos\left(\frac{2\pi(doy - 28)}{365.25}\right) \right) \dots - H \left( \beta_{avg} - \beta_{amp} \cos\left(\frac{2\pi(doy - 28)}{365.25}\right) \right), \quad (13)$$

where  $T$  is the surface temperature measurement,  $T_{avg}$  and  $T_{amp}$  are the MSL temperature yearly average and amplitude, respectively, and  $\beta_{avg}$  and  $\beta_{amp}$  are the temperature lapse rate yearly average and amplitude, respectively. Using this function yields the partial derivatives:

$$\frac{\partial T}{\partial T_{avg,i}} = \frac{\partial T}{\partial T_{avg,p}} \frac{\partial T_{avg,p}}{\partial T_{avg,i}} = \frac{\partial T_{avg,p}}{\partial T_{avg,i}}, \quad (14)$$

$$\begin{aligned} \frac{\partial T}{\partial T_{amp,i}} &= \frac{\partial T}{\partial T_{amp,p}} \frac{\partial T_{amp,p}}{\partial T_{amp,i}} \\ &= -\cos\left(\frac{doy - 28}{365.25}\right) \frac{\partial T_{amp,p}}{\partial T_{amp,i}}, \end{aligned} \quad (15)$$

$$\frac{\partial T}{\partial \beta_{avg,i}} = \frac{\partial T}{\partial \beta_{avg,p}} \frac{\partial \beta_{avg,p}}{\partial \beta_{avg,i}} = -H \frac{\partial \beta_{avg,p}}{\partial \beta_{avg,i}}, \quad (16)$$

$$\begin{aligned} \frac{\partial T}{\partial T_{amp,i}} &= \frac{\partial T}{\partial \beta_{amp,p}} \frac{\partial \beta_{amp,p}}{\partial \beta_{amp,i}} \\ &= H \cos\left(\frac{doy - 28}{365.25}\right) \frac{\partial \beta_{amp,p}}{\partial \beta_{amp,i}}, \end{aligned} \quad (17)$$

where  $T$  is the surface temperature, the subscript  $p$  stands for parameters at the point of interest (not to be confused with  $p$  representing longitude difference and  $P$  representing pressure) and the subscript  $i$  stands for parameters at the grid node  $i$ . Partial derivatives of point values with respect to grid node values (e.g.,  $\frac{\partial T_{avg,p}}{\partial T_{avg,i}}$ ) are evaluated as follows:

$$\begin{aligned} \frac{\partial X_p}{\partial X_1} &= (1-p)(1-q), & \frac{\partial X_p}{\partial X_2} &= p(1-q) \\ \frac{\partial X_p}{\partial X_3} &= q(1-p) \quad \text{and} \quad \frac{\partial X_p}{\partial X_4} &= pq \end{aligned} \quad (18)$$

The derivatives in (18) are used in all steps ( $T$ ,  $P$ ,  $RH$ ) of the adjustments of the grids. Note that these partial derivative elements of point values with respect to grid-node values can be identified in the equations related to temperature, relative humidity, and pressure by the use of the subscripts  $p$  and  $i=1..4$ , as in  $\frac{\partial T_{avg,p}}{\partial T_{avg,i}}$ .

The design matrix for the temperature grid calibration is built according to:

$$\mathbf{A} = \begin{bmatrix} \frac{\partial T^1}{\partial T_{avg,i}} & \frac{\partial T^1}{\partial T_{amp,i}} & \frac{\partial T^1}{\partial \beta_{avg,i}} & \frac{\partial T^1}{\partial \beta_{amp,i}} \\ \vdots & \vdots & \vdots & \vdots \\ \frac{\partial T^n}{\partial T_{avg,i}} & \frac{\partial T^n}{\partial T_{amp,i}} & \frac{\partial T^n}{\partial \beta_{avg,i}} & \frac{\partial T^n}{\partial \beta_{amp,i}} \end{bmatrix}, \quad (19)$$

where the superscripts 1 and  $n$  stand for the observation index (therefore,  $\mathbf{A}$  is a matrix with  $n$  rows, for  $n$  observations). In case the lapse rates are not being adjusted, the design matrix has only two columns (the first two of Equation (19)). The misclosure vector is computed according to:

$$w_i = T^i - T^{i'}, \quad (20)$$

where  $T$  is the measured surface temperature and  $T'$  is the evaluated surface temperature according to (13).

After the temperature grid is calibrated (meaning values of  $T_{avg}$ ,  $T_{amp}$ ,  $\beta_{avg}$  and  $\beta_{amp}$  have been established for all of the grid nodes) the relative humidity grid can be adjusted, or alternatively the pressure grid, which does not depend on temperature or relative humidity.

The ISH Database provides hourly measurements of MSL barometric pressure, no matter the height of the meteorological station. The consequence of this is that the pressure measurements have no relation to any lapse-rate-type parameter. In the case of surface pressure, the respective lapse rate would be  $\beta$ , assuming the height variation of pressure relates to the temperature variation of pressure according to:

$$P_s = P_0 \left( 1 - \frac{\beta H}{T_0} \right)^{\frac{g}{R\beta}} = P_0 \left( \frac{T}{T_0} \right)^{\frac{g}{R\beta}}, \quad (21)$$

where  $P_s$  stands for site pressure. However, because the pressure measurements are related to mean sea level, the function model of the pressure grid adjustment becomes:

$$P_0 = P_{avg} - P_{amp} \cos\left(\frac{2\pi(doy - 28)}{365.25}\right), \quad (22)$$

where  $P_0$  is the MSL pressure measurement and the yearly variation parameters ( $P_{avg}$  and  $P_{amp}$ ) are similar to the ones previously used for  $T$  and  $\beta$  (Eq. (13)). Partial derivatives are also evaluated similarly to (14) and (15):

$$\frac{\partial P_0}{\partial P_{avg,i}} = \frac{\partial P_0}{\partial P_{avg,p}} \frac{\partial P_{avg,p}}{\partial P_{avg,i}} = \frac{\partial P_{avg,p}}{\partial P_{avg,i}}, \quad (23)$$

$$\begin{aligned} \frac{\partial P_0}{\partial P_{amp,i}} &= \frac{\partial P_0}{\partial P_{amp,p}} \frac{\partial P_{amp,p}}{\partial P_{amp,i}} \\ &= -\cos\left(\frac{2\pi(doy - 28)}{365.25}\right) \frac{\partial P_{amp,p}}{\partial P_{amp,i}} \end{aligned} \quad (24)$$

The design matrix then yields:

$$\mathbf{A} = \begin{bmatrix} \frac{\partial P_0^1}{\partial P_{avg,i}} & \frac{\partial P_0^1}{\partial P_{amp,i}} \\ \vdots & \vdots \\ \frac{\partial P_0^n}{\partial P_{avg,i}} & \frac{\partial P_0^n}{\partial P_{amp,i}} \end{bmatrix}, \quad (25)$$

and the misclosure vector is computed according to:

$$w_i = P_0^i - P_0', \quad (26)$$

where  $P_0$  is the measured MSL pressure and  $P_0'$  is the evaluated MSL pressure according to (22).

The calibration of the relative humidity grid involves a little more complexity than the previous ones because (a) it depends on temperature and pressure grids; and (b) the measurements are surface dew point temperature, but the height variation is modeled for water vapor pressure and the yearly variation is modeled for relative humidity. The transformation between these three types of parameters needs to be carried out and incorporated in the functional model for the grid adjustment. The first part of the functional model is the computation of the MSL relative humidity, carried out in a similar manner as for  $T$  and  $P$ :

$$RH_0 = RH_{avg} - RH_{amp} \cos\left(\frac{doy - 28}{365.25}\right), \quad (27)$$

where  $RH_0$  stands for MSL relative humidity and the subscripts “avg” and “amp” stand for yearly average and amplitude, respectively. The relative humidity must then be transformed to water vapor pressure, which will be used for height variation modeling. The relation between the two (relative humidity and water vapor pressure) is given by the following equation [8]:

$$e_0 = RH_0 \cdot es_0 \cdot f_{w,0}, \quad (28)$$

where  $e_0$  is the MSL water vapor pressure,  $es_0$  is the saturation water vapor pressure, and  $f_{w,0}$  is the enhancement factor (both for MSL). Values for  $es_0$  and  $f_{w,0}$  can be computed according to:

$$\begin{aligned} es_0 = & 0.01 \cdot \exp(1.2378847 \times 10^{-5} T_0^2 \\ & - 1.9121316 \times 10^{-2} T_0 + 33.93711047 \\ & - 6.3431645 \times 10^3 T_0^{-1}), \end{aligned} \quad (29)$$

and

$$\begin{aligned} f_{w,0} = & 1.00062 + 3.14 \times 10^{-6} P_0 \\ & + 5.6 \times 10^{-7} (T_0 - 273.15)^2. \end{aligned} \quad (30)$$

The relation between MSL and surface water vapor pressure is expressed using the same physical assumption as in (3), as follows:

$$e = e_0 \left(1 - \frac{\beta H}{T_0}\right)^{\frac{\lambda' g}{R\beta}}, \quad (31)$$

where  $e$  stands for surface water vapor pressure. The last part of the functional model is the relation between  $e$  and dew point temperature, which

can be derived from basic thermodynamic laws, resulting in:

$$e = es(T_d) \cdot f_{w,s}, \quad (32)$$

where  $es(T_d)$  is the saturation water vapor pressure for the dew point temperature  $T_d$ , and can be computed from (29) substituting  $T_d$  for  $T_0$ .  $f_{w,s}$  can be computed from (30) substituting in values of surface pressure and surface temperature. After putting (28) to (32) together, the complete functional model “observation equation” for relative humidity calibration becomes:

$$es(T_d) = RH_0 \cdot es_0 \cdot \frac{f_{w,0}}{f_{w,s}} \cdot \left(1 - \frac{\beta H}{T_0}\right)^{\frac{g\lambda'}{R\beta}}, \quad (33)$$

where, as before, subscripts  $s$  and  $0$  stand for surface and MSL values, respectively. In order to introduce average and amplitude for the modeled parameters in (33),  $RH_0$  is replaced by the right hand side of (27) and  $\lambda'$  is replaced by:

$$\lambda' = \lambda'_{avg} - \lambda'_{amp} \cos\left(\frac{doy - 28}{365.25}\right). \quad (34)$$

The partial derivatives can then be evaluated as (please note that the terms in  $X$  have been described in (18)):

$$\begin{aligned} \frac{\partial es(T_d)}{\partial RH_{avg}} = & \frac{\partial es(T_d)}{\partial RH_{avg,p}} \frac{\partial RH_{avg,p}}{\partial RH_{avg,i}} = \\ & es_0 \cdot \frac{f_{w,0}}{f_{w,s}} \cdot \left(1 - \frac{\beta H}{T_0}\right)^{\frac{g\lambda'}{R\beta}} \cdot \frac{\partial X_p}{\partial X_i} \end{aligned} \quad (35)$$

$$\begin{aligned} \frac{\partial es(T_d)}{\partial RH_{amp}} = & \frac{\partial es(T_d)}{\partial RH_{amp,p}} \frac{\partial RH_{amp,p}}{\partial RH_{amp,i}} = \\ & - \cos\left(\frac{2\pi(doy - 28)}{365.25}\right) \cdot \frac{\partial es(T_d)}{\partial RH_{avg}} \end{aligned} \quad (36)$$

$$\begin{aligned} \frac{\partial e_s(T_d)}{\partial \lambda'_{avg}} = & \frac{\partial e_s(T_d)}{\partial \lambda'_{avg,p}} \frac{\partial \lambda'_{avg,p}}{\partial \lambda'_{avg,i}} = \\ & RH_0 \cdot es_0 \cdot \frac{f_{w,0}}{f_{w,s}} \cdot \left(1 - \frac{\beta H}{T_0}\right)^{\frac{g\lambda'}{R\beta}} \cdot \frac{g}{R\beta} \cdot \\ & \ln\left(1 - \frac{\beta H}{T_0}\right) \cdot \frac{\partial X_p}{\partial X_i} \end{aligned} \quad (37)$$

and

$$\begin{aligned} \frac{\partial e_s(T_d)}{\partial \lambda'_{amp}} = & \frac{\partial e_s(T_d)}{\partial \lambda'_{amp,p}} \frac{\partial \lambda'_{amp,p}}{\partial \lambda'_{amp,i}} = \\ & - \cos\left(\frac{doy - 28}{365.25}\right) \cdot \frac{\partial e_s(T_d)}{\partial \lambda'_{avg}} \end{aligned} \quad (38)$$

and the design matrix becomes:

$$\mathbf{A} = \begin{bmatrix} \frac{\partial e_s(T_d)^1}{\partial RH_{avg,i}} & \frac{\partial e_s(T_d)^1}{\partial RH_{amp,i}} & \frac{\partial e_s(T_d)^1}{\partial \lambda'_{avg,i}} & \frac{\partial e_s(T_d)^1}{\partial \lambda'_{amp,i}} \\ \vdots & \vdots & \vdots & \vdots \\ \frac{\partial e_s(T_d)^n}{\partial RH_{avg,i}} & \frac{\partial e_s(T_d)^n}{\partial RH_{amp,i}} & \frac{\partial e_s(T_d)^n}{\partial \lambda'_{avg,i}} & \frac{\partial e_s(T_d)^n}{\partial \lambda'_{amp,i}} \end{bmatrix}. \quad (39)$$

The misclosure vector is computed according to:

$$w_i = \left( e_s(T_d)^i \right) - \left( e_s(T_d)^{i'} \right), \quad (40)$$

where  $e_s(T_d)$  is computed according to (30) using the measured dew point temperature and  $e_s(T_d)^{i'}$  is evaluated using (34). In case the lapse-rate parameter ( $\lambda'$ ) is not being adjusted, the design matrix has only the two first columns (related to  $RH$ ) and  $\lambda'$  values from UNB3m are used as known values.

#### WIDE AREA MODEL FOR NORTH AMERICA – UNBw.na

In this section, the creation of a model for North America using the previously described procedure is discussed. The model is called UNBw.na, where  $w$  stands for wide area and  $na$  stands for North America. The grid was defined between latitudes 0 and 90 degrees, and (east) longitudes between  $-180$  and  $-40$  degrees, with spacing of 5 degrees in the two directions. Figure 4 shows the North American grid.

The grid is first initialized with UNB3m values, and then the grid node values are updated (adjusted) using the previously described approach. The initialization of the grid is fundamental for its adjustment because meteorological stations in the ISH Database do not cover every cell of the grid. In this case, the grid node receives no update, and the consequence is a value equal to UNB3m's. The stations to be used in the calibration of the grid were chosen simply taking database stations

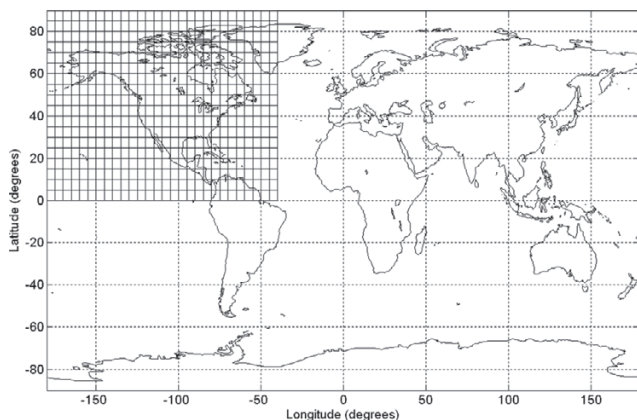


Fig. 4–UNBw.na grid.

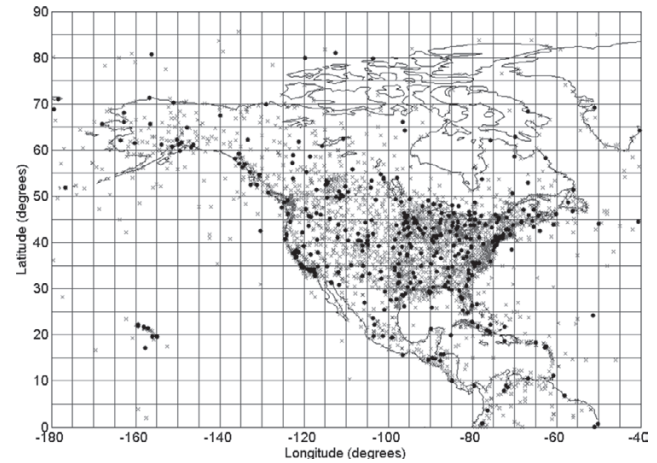


Fig. 5–Distribution of the control stations (dots) and the calibration stations (crosses).

within the grid boundaries (in this case a total of around 4000 stations). Figure 5 shows the distribution of meteorological stations over the grid.

In order to access the grid adjustment, 400 stations were randomly separated from the dataset to be used as control stations. The data from these stations was not used in the grid calibration, and after each adjustment step they were used to check results obtained for temperature, pressure, and water vapor pressure. Figure 5 also shows the distribution of the control stations (dots) and calibration stations (crosses).

#### Temperature Calibration

As shown in the previous section, the temperature lapse rate and water vapor pressure height factor could be calibrated or not. The two approaches were tested for this data set, and it turned out that the model provided slightly better results when lapse rates from UNB3m were used as known and were not recalibrated. One of the reasons which could have caused this is the fact that stations within a given grid cell have similar heights, which causes difficulties in the decorrelation between temperature or water vapor pressure and their lapse-rate parameters (since the former two are functions of lapse rates and heights – see, e.g., (12) and (31)). Figure 6 shows the height (represented by grayscale) of the stations, where it is possible to notice that apart from a few cells, the height of stations inside cells is usually very similar.

The following results are presented only for the case when the lapse rates were not calibrated. Figure 7 shows a representation of average MSL temperature given by UNB3m and UNBw.na for all grid nodes of the model. It is possible to notice that UNBw.na shows lower temperatures for some northern regions. Also, for some regions, the

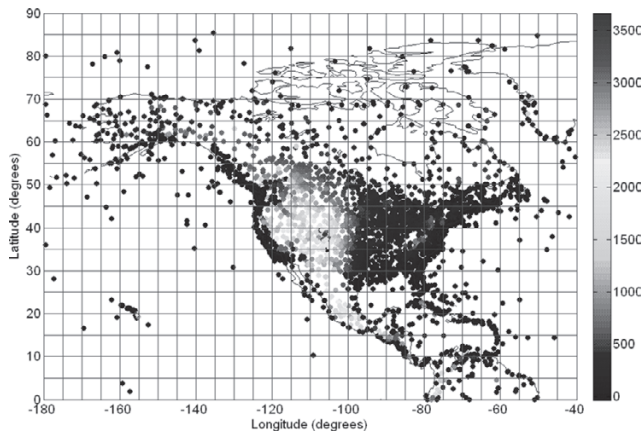


Fig. 6—Height (in meters – represented by grayscale) of the meteorological stations.

temperature does not quite follow a variation dependent on latitude only. The two grids are practically the same for grid nodes outside continental areas (over seas) because there is not enough data for grid calibration in these regions (see Figure 5), and UNB3m values from the initialization are almost unmodified by the calibration process.

Figure 8 shows the difference between the two models, in the sense of UNBw.na-UNB3m. It can be seen that UNBw.na provides higher temperatures over the western part of North America, and lower temperatures for land mass regions with higher latitudes over the eastern part of the continent.

By using the two models to estimate the temperature for control stations, it is possible to check if these differences improve the model or not. Figure 9 shows the biases encountered when estimating temperatures for control stations, using the two models, in the sense of modeled value – observed value. It is possible to notice that there is a significant

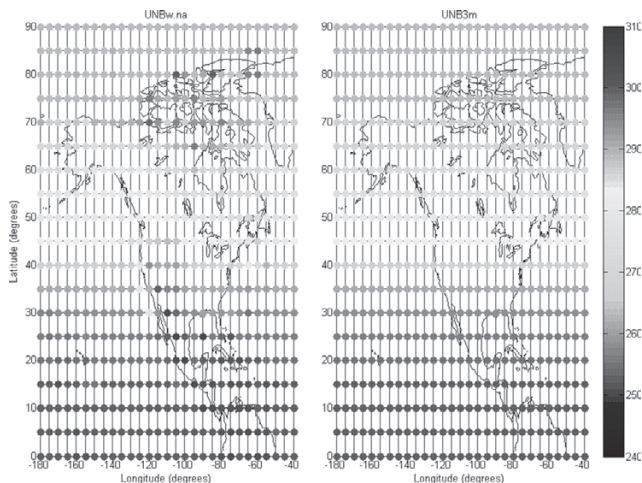


Fig. 7—Average MSL temperature given by UNB3m and UNBw.na, in kelvins.

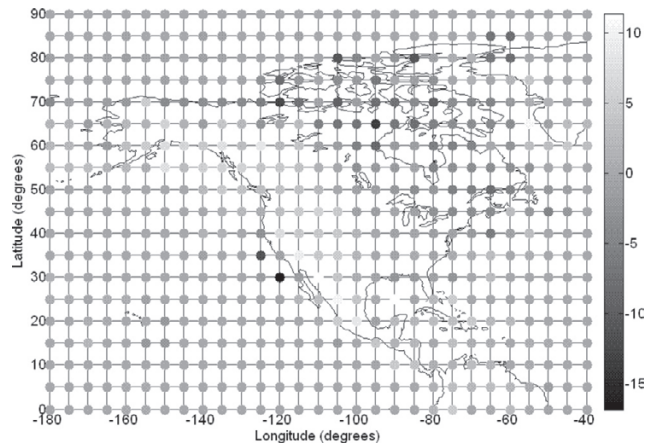


Fig. 8—MSL temperature difference between UNBw.na and UNB3m, in kelvins.

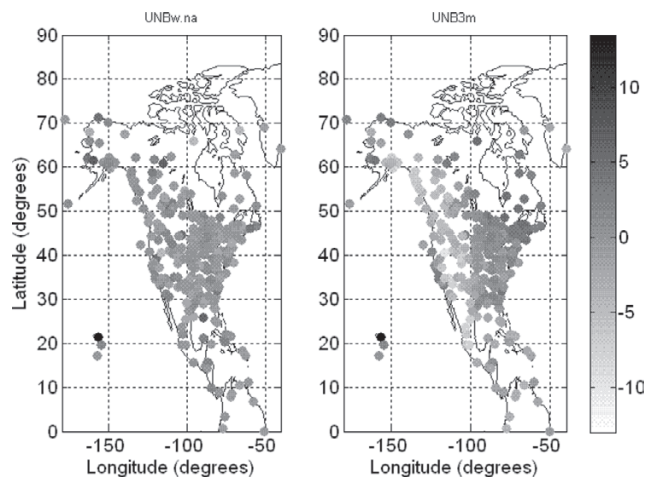


Fig. 9—Biases encountered when estimating temperature for control stations, in kelvins.

improvement in estimation for stations in the western part of North America, matching with differences of grid values (Figure 8) for the same region. UNB3m slightly overestimates the temperature for a localized region near the east coast. For UNBw.na, there is no trend related to longitude variation.

General statistics for temperature estimation errors for the two models with respect to control station values are given in Table 2, where the overall improvement in temperature estimation brought by UNBw.na is clear. The values in Table 2 (and similar tables for pressure and water

Table 2—General Statistics for Temperature Estimation Errors (All Values in kelvins)

	Bias	Std. Dev.	RMS
UNBw.na	0.06	5.57	5.80
UNB3m	-0.68	6.04	6.80

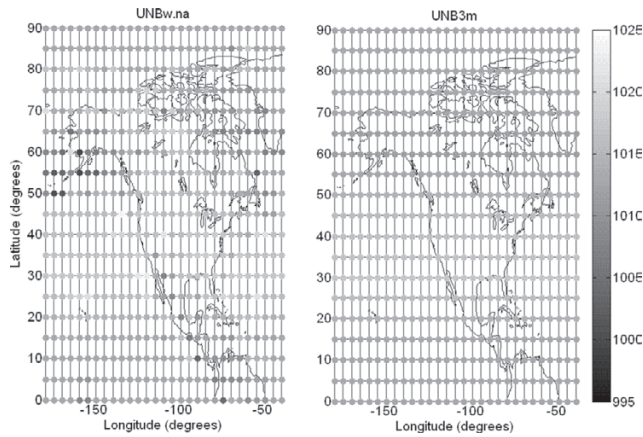


Fig. 10—Average pressure at grid nodes, given by UNBw.ca and UNB3m, in mbar.

vapor to be shown later) were computed using one value (bias, standard deviation, and rms) per station, regardless of the number of measurements available for each station. There is a significant improvement in the bias of the model (91%), showing that UNB3m generally underestimates the mean temperature. This systematic behavior is dominated by the temperature underestimation over the western part of the continent.

### Pressure Calibration

The results of the pressure grid calibration are shown in Figure 10, where it can be seen that UNBw.ca, unlike UNB3m, is not simply latitude dependent. Figure 11 shows the difference between average MSL pressure of the two models, in the sense of UNBw.ca-UNB3m. It can be noticed that the major differences are encountered in regions situated in the northwest, northeast and southern parts of the continent. Differences vary by up to around 10 mbar, which means a difference of

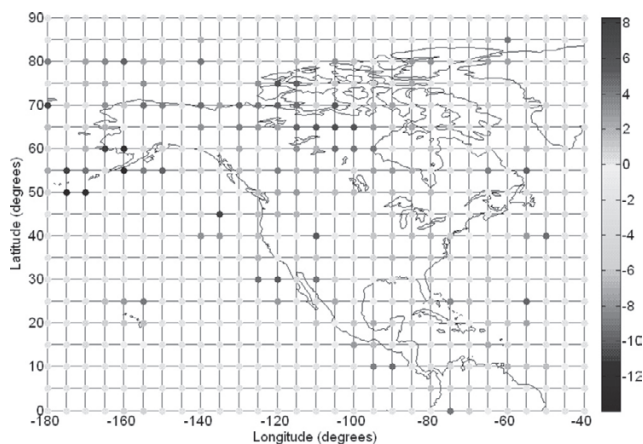


Fig. 11—Average MSL pressure difference between UNBw.ca and UNB3m, in mbar.

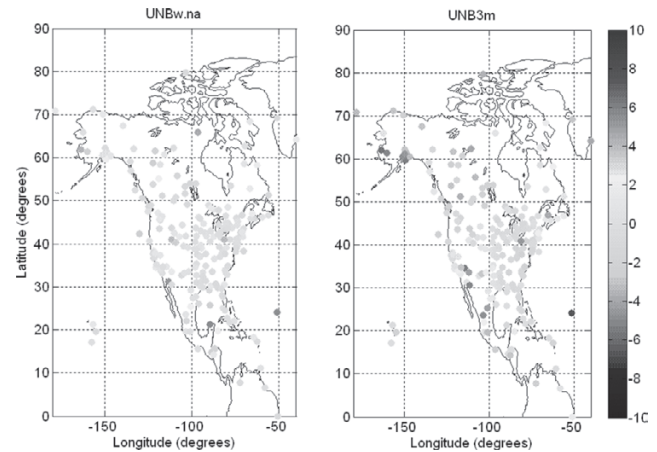


Fig. 12—Mean biases encountered when estimating pressure for control stations, in mbar.

around 2 cm in hydrostatic delay estimation (according to Equation (2), if we consider a point at MSL with the delay rate with respect to pressure value around 0.0022 m/mbar). Figure 12 shows the biases of UNB3m and UNBw.ca when estimating pressure for the control stations, where it can be seen that UNBw.ca performs better than UNB3m for the regions where greater differences are found. Overall, the bias plot of UNBw.ca is lighter than UNB3m's, which means it is usually closer to zero (lighter gray on the grayscale).

The general statistics for pressure estimation are shown in Table 3.

From Table 3 it can be noticed that the differences for bias, standard deviation, and rms between the two models are low (considering estimated delays, 1 mbar corresponds to around 2 mm in the zenith direction). Although the general bias of UNBw.ca is slightly worse than UNB3m's, it is statistically insignificant. Furthermore, UNBw.ca's better fitting for different regions is translated into an improvement in standard deviation and rms.

### Relative Humidity Calibration

The last step of the model calibration is the relative humidity grid. Following the same procedure as for the other two steps in terms of reporting results, Figure 13 shows the average MSL values of *RH* (in %) for all grid nodes, given by UNBw.ca and UNB3m, where it can be seen that UNBw.ca shows a drier area in the southwest part of the

Table 3—General Statistics for Pressure Estimation Errors (All Values in mbar)

	Bias	Std. Dev.	RMS
UNBw.ca	0.05	3.89	3.95
UNB3m	0.02	3.95	4.12

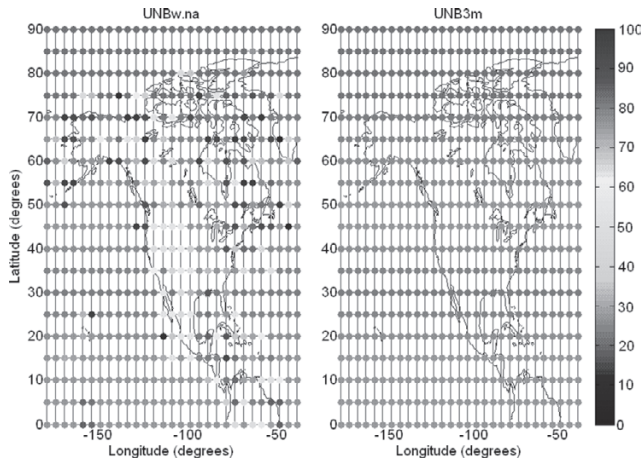


Fig. 13—Average MSL relative humidity for grid nodes, given by UNBw.na and UNB3m, in %.

continent. This difference can be better visualized in Figure 14, which shows the difference in the average MSL values between the two models for each grid node, in the sense of UNBw.na-UNB3m (in %).

The biases of the water vapor pressure estimation for control stations are shown in Figure 15, where we can notice that UNB3m overestimates the water vapor pressure for the southwest part of the continent, while UNBw.na does not. There is also a region with a small improvement in the northwest part of the continent (in this last case, UNB3m underestimates the water vapor pressure).

The general performance results can be seen in Table 4, where it can be noticed that there is a significant improvement (around 50%) in bias when estimating surface water vapor pressure with UNBw.na as compared to UNB3m. There is a small improvement in standard deviation, indicating a slightly better fitting to real conditions by UNBw.na.

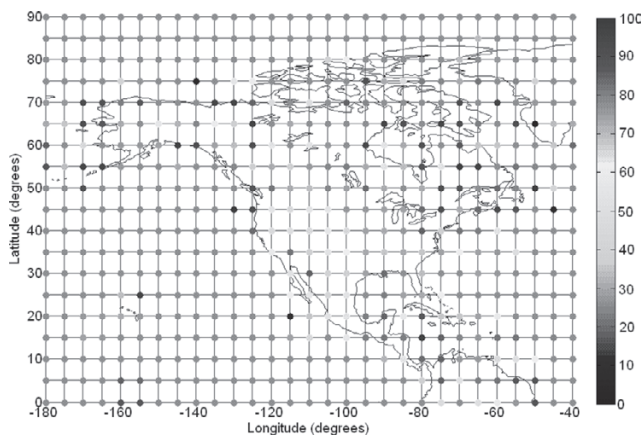


Fig. 14—Difference between average MSL relative humidity provided by UNBw.na and UNB3m, in %.

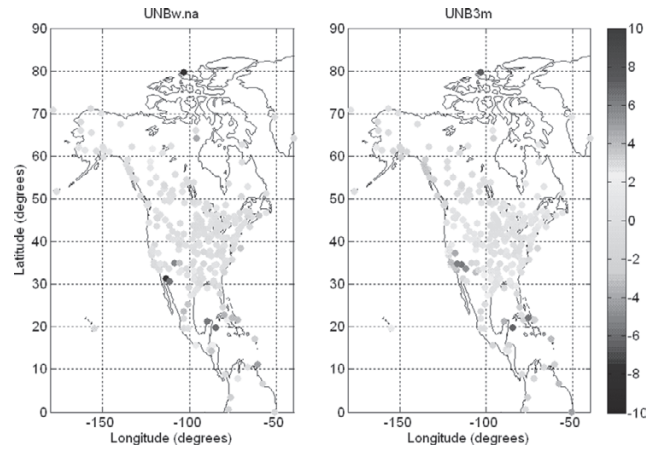


Fig. 15—Mean biases encountered when estimating water vapor pressure for control stations, in mbar.

Table 4—General Statistics for Water Vapor Pressure Estimation Errors (All Values in mbar)

	Bias	Std. Dev.	RMS
UNBw.na	-0.10	2.30	2.47
UNB3m	0.20	2.43	2.65

#### UNBw.na VALIDATION WITH RAY-TRACED DELAYS

In order to verify if UNBw.na is more realistic than UNB3m in terms of delay estimation, a validation process was realized. In this approach radiosonde-derived delays were used as reference (“truth”). The radiosonde profiles of temperature, pressure, and dew point temperature were used to compute zenith delays by means of a ray-tracing technique. We used radiosonde soundings taken throughout North America and some neighboring territories over the years 1990 to 1996 inclusive. A total of 222 stations were used, distributed as shown in Figure 16.

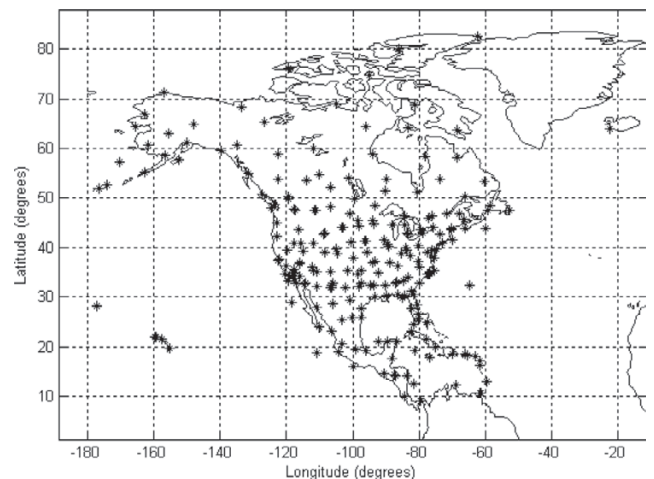


Fig. 16—Distribution of radiosonde stations in North America and some nearby territories.

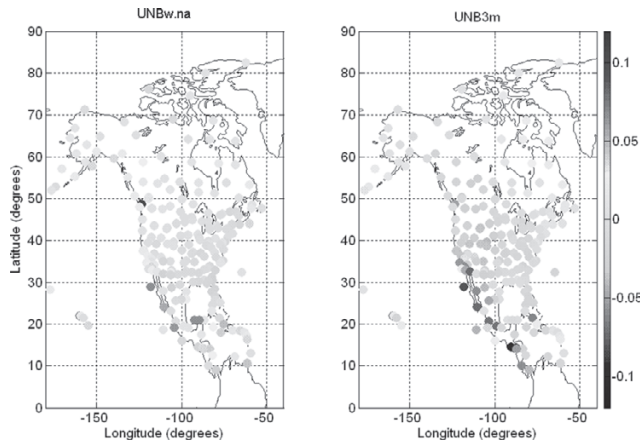


Fig. 17—Total zenith delay estimation biases for each station, in meters.

Each station usually launched a balloon twice a day, totaling 701,940 soundings for all stations, throughout the seven years. For each one of the soundings, a total zenith delay was predicted using UNBw.na and UNB3m, and then compared with the ray-traced total zenith delays. From this comparison, bias and rms values could be computed for each one of the stations shown in Figure 16. Figure 17 shows the mean biases found for all stations with the two models.

In Figure 17, the zero value is very light gray according to the grayscale. It is possible to notice that the UNBw.na plot shows shades generally closer to very light gray than UNB3m. It can also be noticed that in the western part of the continent, where UNB3m has its worse performance, there is a significant improvement with the new model. The rms values for the same stations can be seen in Figure 18, where it is possible to see that the UNBw.na plot presents generally lighter shades of gray (in this plot zero is represented by white), also with good improvement for the region with worst results provided by UNB3m.

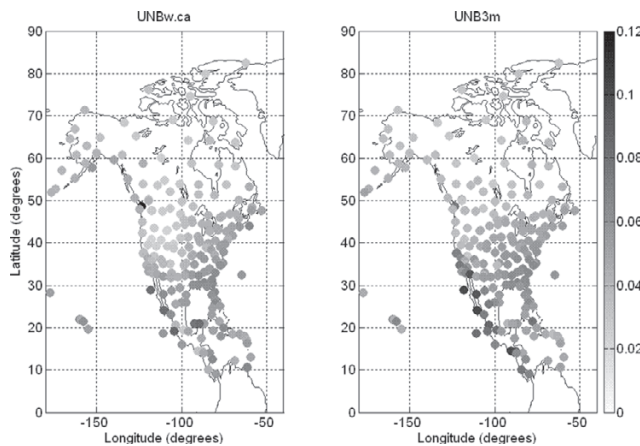


Fig. 18—Total zenith delay estimation rms values for each station, in meters.

Table 5—General Statistics of Total Zenith Delay Prediction Performance (All Values in mm)

	Bias	Std. Dev.	RMS
UNBw.na	3.6	44.8	45.0
UNB3m	-5.2	48.9	49.2

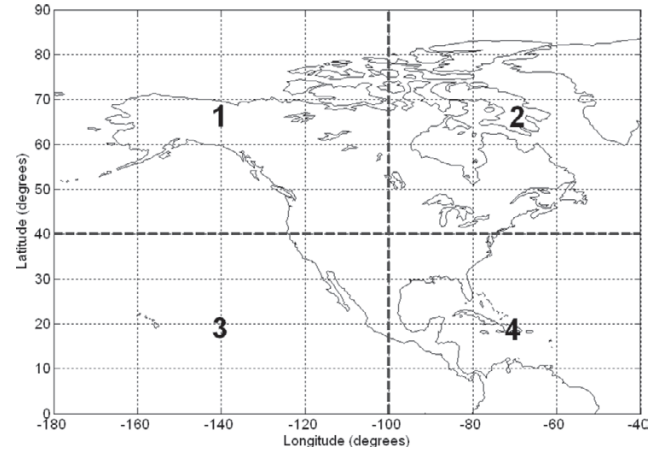


Fig. 19—Division of the four analysis regions.

The general statistics of delay prediction performance of the two models are shown in Table 5, where we can see that there is a general improvement of absolute bias of around 30%, and small improvements in standard deviation (8%) and rms (9%).

Although the general rms doesn't show a significant improvement, the major concern with UNB3m is not its overall performance, but its performance in localized areas. In order to assess the performance of the models in different regions, the coverage area was divided into four analysis regions, trying to have approximately the same number of radiosonde stations in each one of them. Figure 19 shows the division of the four regions.

The statistics for each one of the analysis regions are shown in Table 6.

In Table 6 it can be noticed that rms values for UNBw.na are better than UNB3m's for all regions, with a significant improvement for Region 3 (around 23%). The bias of Region 3 for UNBw.na is higher than for UNB3m; however it does not mean

Table 6—Statistics (Bias, Standard Deviation, and RMS) for Analysis Regions (All Values in cm)

Station	UNBw.na			UNB3m		
	Bias	SD	RMS	Bias	SD	RMS
1	1.0	3.4	3.6	-0.9	3.5	3.7
2	0.4	4.1	4.1	0.5	4.3	4.3
3	0.6	4.4	4.4	0.2	5.7	5.7
4	-0.3	5.4	5.5	-1.3	5.6	5.8

Table 7—Average Absolute Biases (aab) and Their Standard Deviations (aab-sd) – All Values in cm

Region	UNBw.na		UNB3m	
	aab	aab-sd	aab	aab-sd
1	2.8	2.2	2.8	2.3
2	3.2	2.6	3.4	2.7
3	3.4	2.9	4.5	3.6
4	4.5	3.2	4.7	3.4

UNB3m is better, because although the mean bias is less, the variation of biases (above and below zero) is much higher than for UNBw.na (as in Figure 17). This effect shows up in UNB3m's standard deviation and rms in Region 3, which are significantly higher than UNBw.na's. Another way to show that is by computing the average absolute biases and their standard deviation, computed without considering bias sign. These values are shown in Table 7, where it can be noticed that, indeed, the average absolute bias and its standard deviation are significantly higher for UNB3m in Region 3 (UNBw.na shows an improvement of around 25%).

One of the problems encountered in previous UNB neutral atmosphere models is a systematic behavior with respect to height [1]. In order to verify if the new model has the same problem, Figure 20 shows a plot of the delay biases at the radiosonde stations with respect to station heights. The error bars are (one sigma) standard deviations of the bias computation for each of the stations, and the line is the fitted (using the points shown in the plots) linear trend of the models. The upper plot shows results of UNBw.na and the lower one shows UNB3m's results.

It can be seen in Figure 20 that UNBw.na does not have a trend as significant as UNB3m, because while UNB3m biases tend to increase negatively with increasing height, UNBw.na biases stay close

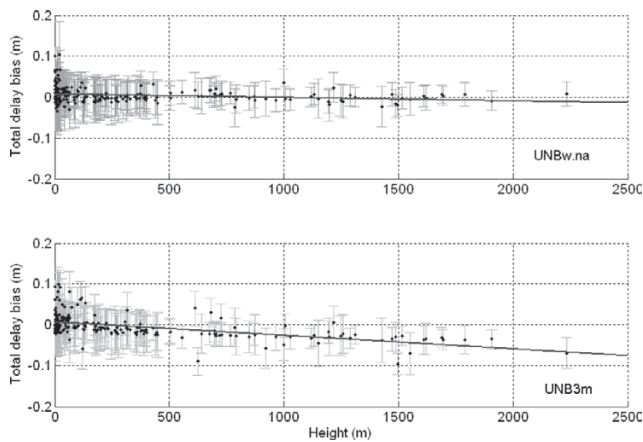


Fig. 20—Station biases with respect to station heights.

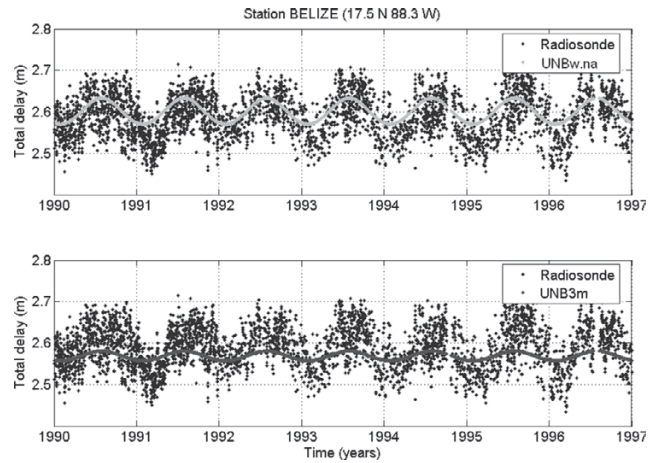


Fig. 21—Total zenith delay estimation for station Belize.

to zero no matter the height of the station. This difference can also be clearly seen comparing the two trend lines of the models. One potential reason for the improvement with respect to height variation is the fact that the grid calibration procedure optimizes the model for points near the topographic surface, where the data used for the calibration was observed.

In order to visualize the fit of the model estimations to the yearly variation of the zenith total delay, a few stations were selected for analysis.

The station selection was based on availability of data for given stations over the period of time of the data set 1990-1996, having sample stations for different latitudes. The chosen stations are Belize (City), Belize; Pittsburgh, PA, U.S.A.; Salt Lake City, UT, U.S.A.; Bethel, AK, U.S.A.; and Eureka, Nunavut, Canada. Figures 21 to 25 show the radiosonde ray-traced total zenith delays compared with UNB3m and UNBw.na predictions for each of the stations.

The estimations provided by UNB3m for station Belize have a problem with the annual amplitude

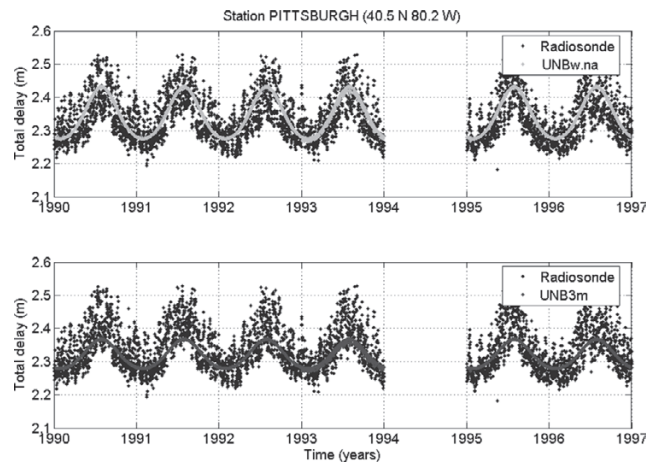


Fig. 22—Total zenith delay estimation for station Pittsburgh.

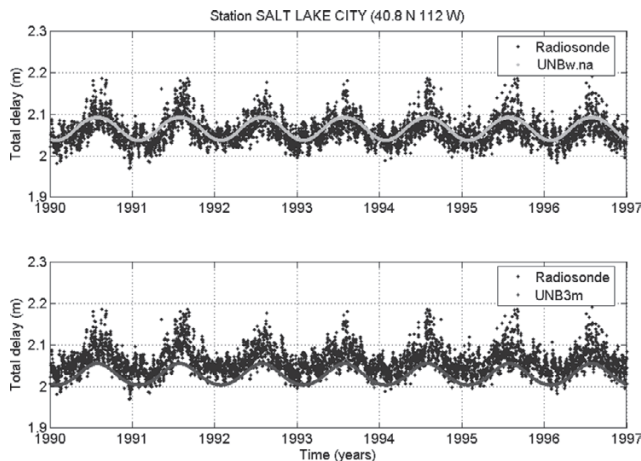


Fig. 23—Total zenith delay estimation for station Salt Lake City.

of the delays. This effect is caused by the fact that UNB3m assumes that meteorological parameters do not vary over the year for latitudes between 15°N and 15°S. The problem with amplitude underestimation affects even stations at higher latitudes, as in the case of station Pittsburgh. UNBw.na shows good improvement in terms of estimated annual amplitude, as can be seen for these two stations.

Another problem suffered by UNB3m in the case of Pittsburgh is the underestimation of the delays, which also occurs for Salt Lake City. The average of the delays provided by UNBw.na seem to match much better with ray-traced delays than UNB3m's for these stations. The plot for station Pittsburgh has a gap because there was no radiosonde data available for 1994 in the dataset provided.

In the case of station Bethel, both models seem to work fine, with a good fit with radiosonde-derived delays. However, for the northern station, Eureka (80°N), UNB3m predictions generally overestimate the delays, while UNBw.na is closer to

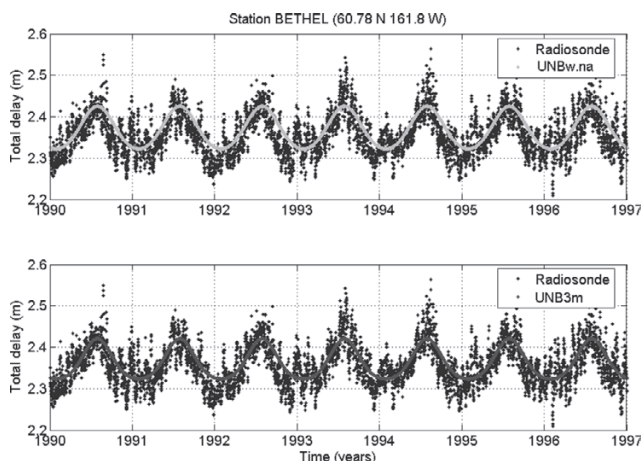


Fig. 24—Total zenith delay estimation for station Bethel.

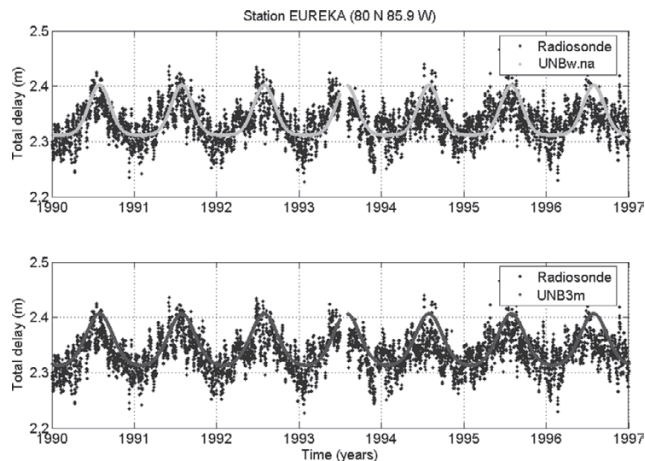


Fig. 25—Total zenith delay estimation for station Eureka.

the average values of the ray-traced delays over the years.

Table 8 shows the numerical results for each of the five stations. With the exception of station Bethel, UNBw.na shows better results for all stations, with improvement of up to 2.8 cm in bias and 1.6 cm in rms (both for station Salt Lake City). If the biases for all stations are considered, it is possible to notice that UNBw.na has more consistent (homogeneous) results for different locations.

## CONCLUSIONS AND FUTURE WORK

In this paper, we have comprehensively described and demonstrated an approach for creation of wide area neutral atmosphere models. A multi-year dataset with hourly surface meteorological measurements was used to create a new model for North America, called here UNBw.na.

The calibration of surface temperature and water vapor pressure lapse-rate parameters was performed, and after comparing results to a model calibration with fixed lapse rates it was concluded that better performance is achieved in the latter case. One of the reasons behind this conclusion

Table 8—Numerical Results for Sample Stations (Represented by the First Four Characters of Their Names) — All Values in cm

Station	UNBw.na		UNB3m	
	Bias	RMS	bias	RMS
BELI	1.4	4.7	2.1	5.3
PITT	0.6	4.7	-1.8	5.3
SALT	0.5	2.6	-3.3	4.2
BETH	1.2	3.8	0.6	3.6
EURE	0.5	2.9	1.5	3.2

might be the fact that the current dataset (surface meteorological parameters) is not adequate for successfully decorrelating surface lapse rates from actual parameters, due to fact that stations nearby each other tend to have similar heights.

The meteorological values derived from the grids of the new model were compared with actual surface measurements, realized at stations which were not used in the calibration process. All analyses took into consideration the most recent version of UNB models, until now UNB3m.

Results for all three meteorological parameters showed that a grid-based model could perform better than a latitude-only based model, such as UNB3m. The reason for that is the capability of accommodating longitudinal or regional climatic characteristics of the continent. In terms of temperature, the general bias was practically eliminated, with a reduction of 91% ( $-0.68$  to  $0.06$  K), while rms was improved by 15% ( $6.8$  to  $5.8$  K). Pressure estimations were also improved in the new model, with a reduction of more than 50% in bias ( $0.05$  to  $0.02$  mbar) and a slight improvement in rms ( $4.12$  to  $3.95$  mbar). Water vapor pressure predictions had their general bias reduced 50% ( $0.2$  to  $-0.1$  mbar), also with slight improvement in rms ( $2.65$  to  $2.47$  mbar). Although the general results do not show a spectacular improvement, the new model is consistently better than its predecessor, and the improvement for certain regions, where the performance of the old model was not satisfactory, is significant.

A validation of UNBw.na predicted zenith delays was realized using radiosonde-derived delays as reference. Soundings carried out throughout North America and some neighboring territories over the years 1990 to 1996 inclusive, were used in this analysis, totaling 222 stations. Results from this analysis showed a general improvement of bias of around 30%, and small improvements in standard deviation (8%) and rms (9%).

Because the main goal of the new model is to predict zenith delays with a consistent uncertainty for different areas, the continent was divided into four analysis regions. This was done to detect localized improvements when using UNBw.na. This analysis showed that all regions manifested improvement for the estimations with the new model.

A problem with systematic behavior of biases (of zenith delay estimation) with height which has been previously detected in UNB neutral atmosphere models no longer exists in UNBw.na. Biases were shown to be consistently close to zero, no matter the height of the station.

Investigation of the performance of both models (UNBw.na and UNB3m) with radiosonde ray-traced delays at a few sample stations showed that UNBw.na generally has a better fit to the yearly

behavior of the zenith delays. It was also possible to notice that results from UNBw.na are more consistent between stations at different locations than when using UNB3m.

In terms of general conclusions, UNBw.na was shown to be consistently better than UNB3m in several ways. The adopted procedure for the grid calibration worked well, resulting in a reliable model. Even though the process for creating the grids of the wide area models is reasonably complex, this complexity exists only for the generation of the grid which is a one-time procedure. Once the grid is created, its usage is actually very simple. In fact, the model evaluation is quite similar to UNB3m's look-up table evaluation, with the only difference being that values are interpolated in two dimensions instead of only one. Given today's computing capabilities, even in handheld devices, there is no significant difference in the necessary processing power or array storage requirements between UNBw.na and its predecessor UNB3m.

Future work involves investigation of lapse-rate parameters, which were not calibrated in this work. The model for delay computation, which has not been modified so far, will also be reviewed. Assimilation of different data, such as numerical weather models or contemporary standard atmospheres, still needs to be investigated.

A version of this paper with color graphics is available on line at <http://gge.unb.ca/Research/GRL/UNBw.na.pdf>.

## ACKNOWLEDGEMENTS

We would like to thank Seth Guttman and his colleagues at NOAA for making the ISH Database available to us. We also would like to thank James Davis, Thomas Herring, and Arthur Niell for the ray-tracing software and Paul Collins for providing the radiosonde quality-control software. The authors gratefully acknowledge the financial support of the Canadian International Development Agency. We thank the reviewers for their helpful comments, which have improved the readability of the paper.

An earlier version of this paper was presented at ION GNSS 2006, the 19th International Technical Meeting of the Satellite Division of The Institute of Navigation, Fort Worth, TX, 26–29 September 2006.

## REFERENCES

1. Leandro, R. F., Santos, M. C., and Langley, R. B., *UNB Neutral Atmosphere Models: Development and Performance*, Proceedings of the 19<sup>th</sup> National Technical

- meeting of The Institute of Navigation, Monterey, California, January 18–20, 2006, pp. 564–573.
2. Leandro, R. F., Langley, R. B., and Santos, M. C., *UNB3m\_pack: A Neutral Atmosphere Delay Package for Radiometric Space Techniques*, GPS Solutions, January 2008, Vol. 12, No. 1, DOI 10.1007/s10291-007-0077-5, pp. 65–70.
  3. Davis, J. L., Herring, T. A., Shapiro, I. I., Rogers, A. E. E., and Elgered, G., *Geodesy by Radio Interferometry: Effects of Atmospheric Modeling Errors on Estimates of Baseline Length*, Radio Science, 1985, Vol. 20, No. 6, DOI 10.1029/RS020i006p01593, pp. 1593–1607.
  4. Niell, A. E., *Global Mapping Functions for the Atmosphere Delay at Radio Wavelengths*, Journal of Geophysical Research, 1996, Vol. 101, No. B2, DOI 10.1029/95JB03048, pp. 3227–3246.
  5. Krueger, E., Schüler, T., Hein, G. W., Martellucci, A., and Blarzino, G., *Galileo Tropospheric Correction Approaches Developed within GSTB-V1*, Proceedings of GNSS 2004, the European Navigation Conference, May 17–19, 2004, Rotterdam, The Netherlands.
  6. COESA, *U.S. Standard Atmosphere Supplements, 1966*, U.S. Committee on Extension to the Standard Atmosphere, sponsored by Environmental Science Services Administration, National Aeronautics and Space Administration, United States Air Force and published by the Superintendent of Documents, U.S. Government Printing Office, Washington, D.C., 1966.
  7. Collins, J. P. and Langley, R. B., *The Residual Tropospheric Propagation Delay: How Bad Can It Get?*, Proceedings of the 8<sup>th</sup> International Technical Meeting of The Institute of Navigation, ION GPS-98, Nashville, TN, September 15–18, 1998, pp. 729–738.
  8. McCarthy, D. D. and Petit, G. (eds.), *IERS Conventions (2003)*, International Earth Rotation and Reference Systems Service, Technical Note 32, Verlag des Bundesamts für Kartographie und Geodäsie, Frankfurt am Main, Germany, 2004.